Two-dimensional field-sensing map and magnetic anisotropy dispersion in magnetic tunnel junction arrays

Wenzhe Zhang, Gang Xiao, and Matthew J. Carter

Phys. Rev. B **83**, 144416 — Published 22 April 2011

DOI: 10.1103/PhysRevB.83.144416

Two-dimensional Field Sensing Map and Magnetic Anisotropy Dispersion in Magnetic Tunnel Junction Arrays

Wenzhe Zhang* and Gang Xiao†
Department of Physics, Brown University, Providence, RI 02912

Matthew J. Carter
Micro Magnetics, Inc., 617 Airport Rd., Fall River, MA 02720

Due to the inherent disorder in local structures, anisotropy dispersion exists in almost all systems that consist of multiple magnetic tunnel junctions (MTJs). Aided by micromagnetic simulations based on the Stoner-Wohlfarth (S-W) model, we used a two-dimensional field sensing map to study the effect of anisotropy dispersion in MTJ arrays. First, we recorded the field sensitivity value of an MTJ array as a function of the easy- and hard-axis bias fields, and then extracted the anisotropy dispersion in the array by comparing the experimental sensitivity map to the simulated map. Through a Mean-Square-Error based image processing technique, we found the best match for our experimental data, and assigned a pair of dispersion numbers (anisotropy angle and anisotropy constant) to the array. By varying each of the parameters once at a time, we were able to discover the dependence of field sensitivity on magnetoresistance ratio, coercivity, and magnetic anisotropy dispersion. Effects from possible edge domains are also discussed to account for a correction term in our analysis of anisotropy angle distribution using the S-W model. We believe this model is a useful tool for monitoring the formation and evolution of anisotropy dispersion in MTJ systems, and can facilitate better design of MTJ-based devices.

I. INTRODUCTION

Magnetic tunnel junctions (MTJs) with crystalline tunnel barriers have been extensively studied over the last few years. A tunneling magnetoresistance ratio (TMR) in excess of 200% in such devices has made them excellent candidates for applications in spin-based electronics[1,2]. One of the applications, a magnetoresistive field sensor, is usually configured such that the magnetization of the free layer is perpendicular to that of the pinned layer (pinning axis), either due to biasing magnetic fields[3] or high shape anisotropy[4]. When subjected to a magnetic field along the pinning axis, the magnetization of the free layer undergoes a coherent rotation, yielding an almost linear response on the magnetoresistance. In hope to increase this linearity and to boost the sensor sensitivity to the picotesla scale, several research groups have proposed a variety of techniques: using a single field applied at an angle between the hard and easy axes, P. Pong *et al.*[5] obtained a linear nonhysteretic response in Al_2O_3 based MTJs with a magnetic field sensitivity as high as 13.8%/Oe. The introduction of a second antiferromagnetic thin film adjacent to the detection layer, as reported by Negulescu *et al.*[6], allowed tuning both the sensitivity and the linear range of the MTJ sensor.

As demonstrated by rapidly growing amount of literatures on the subject, the magnetic properties of MTJ devices can be characterized by using the acquired magneto-transport properties, thus revealing the micromagnetics of the free layer, which is often in micron to submicron scales. For instance, Mazumdar *et al.*[7] mapped the magnetic field sensitivity and low-frequency 1/f voltage noise of an MTJ in orthogonal magnetic fields. The so-called noise map uncovered the possible origin of intrinsic magnetic noise of MTJ devices. Safron *et al.*[8] used a circle transfer curve method to determine the magnetic parameters that govern the behavior of MTJ devices. By recording an MTJ device resistance as a function of the applied field angle, information about the free layer's anisotropy orientation can be provided. Although Safron suggested that analysis of an MTJ's remnant resistance curve may yield the dispersion of the free layer anisotropy, they didn't give a quantitative approach.

In Safron's work, the Stoner and Wohlfarth (S-W)[9,10] model was employed to yield theoretical estimations for the anisotropy angle and the anisotropy constant for an MTJ's free layer. The model describes the rotation of the magnetic moment of a single-domain magnetic particle with an anisotropy easy-axis. The S-W model generates both the reversible and irreversible changes in magnetization under a multi-dimensional magnetic field, taking into account the arbitrary strength of magnetic anisotropy. A single MTJ element with a well-defined free layer having a uniaxial anisotropy follows the S-W model relatively well. On the other hand, for an MTJ magnetic sensor array made up of multiple elements, each sensing element has its own anisotropy due to inherent disorder in local structures or the patterning process. The anisotropy parameters of the sensing elements, such as anisotropy-axis and anisotropy constant, are not uniform, yet they satisfy certain statistical distribution. A series of tests have indicated that the dispersion in this type of distribution often acts against achieving good sensitivity. Since the modeling of the magnetic behavior of such a spintronic device is more complicated than what the simple S-W model can predict, developing a more complete model is needed in order to understand the magnetic properties of such systems, and that is the aim of this study.

This paper is arranged in the following manner: first we will determine the magnetic sensitivity by using a two-dimensional field sensing map as described in reference[7], and then we will present a model to account for the anisotropy dispersion. Finally, we will talk about conclusions derived from this model, and its comparison to the experimental work.

II. EXPERIMENTAL METHODS

We deposited MTJ multilayer films on thermally oxidized silicon wafers using a custom multi-target high-vacuum magnetron sputtering system (base pressure of 2×10^{-8} Torr). The MTJ stack has the following structure(thicknesses in angstroms):50Ta/300Ru/50Ta/20CoFe
/150IrMn/20CoFe/8Ru/30CoFeB/19MgO/30CoFeB/50Ta/100Ru. All layers except the MgO barrier were deposited by DC sputtering at a constant Ar pressure of 2.05mTorr. The MgO barrier was deposited by radio frequency (RF) magnetron sputtering at an Ar pressure of 1.1 mTorr. During the sputtering process, the substrates were rotated at a constant speed to maximize uniformity throughout each wafer. Micron-size elliptical junctions were patterned using standard photolithography and ion-beam milling process. A 150-nm-thick gold layer was deposited over the defined junction area and patterned into low resistance top contact leads. The free layers of the junctions studied had lateral dimensions of $50 \times 90\mu m^2$, and the MTJ arrays consisted of thirty-eight free layer elements connected in series with the whole resistance about 2 KΩ.

After deposition and patterning, high temperature magnetic annealing was used to define the intrinsic magnetic axis and to achieve a high magnetoresistance ratio. Typically, the MTJs were annealed at 310°C for 4 hours at 8×10^{-8} Torr in an applied magnetic field of 4.5 KOe. The field was applied along the shorter axis of the free layer oval. After annealing, the magnetic pinning direction of the pinned layer is always parallel to the shorter axis of the free layer. The magnetic anisotropy of the free layer is predominantly due to the magnetocrystalline anisotropy induced by the magnetic annealing. Because of this, the easy-axis of the free layer is in fact the shorter axis.

We performed magnetic sensitivity measurements in orthogonal magnetic fields applied along the easy- (H_E) and hard- (H_B) axis of the MTJ elements. The four-terminal MTJ device was wire-bonded onto a DIP-SOIC (duel inline package-small outline integrated circuit) adapter, and then mounted onto a printed circuit board (PCB) which was connected for four-probe measurements. Two pairs of orthogonally placed electromagnets provided the easy- and hard-axis fields. A pair of Helmholtz coils generated a small AC magnetic field ($\triangle H \sim 1$ Oe) along the easy-axis direction of the MTJ array. The voltage AC output from the MTJ ($\triangle V$), in response to $\triangle H$, was measured by using a lock-in amplifier as a function of H_E and H_B. It is a common practice to express the field sensitivity s in terms of the relative voltage change, *i.e.* $s \equiv (1/V)(dV/dH) = (1/G)(dG/dH)$, where G is the electric conductance, and d is the derivative symbol. By using this setup, we developed the so-called sensitivity map, a technique of mapping the sensitivity value in a two-dimensional orthogonal magnetic field space, in order to extract the relevant sensing and magnetic anisotropic properties of the free layer elements[7].

III. COMPUTATIONAL METHODS

To understand the sensitivity map, we attempted to model a system consisting of a collection of S-W single-domain magnetic particles, with each particle corresponding to one free layer element in our MTJ array. Each element or particle is specified by its magnetic moment ($\boldsymbol{m}_s$), anisotropy constant (K_u), and easy-axis direction (α). Because of the inherent disorder in local structures or due to the patterning process, these parameters are not uniform. However, they satisfy certain statistical distributions. In this study, we ignored any magnetostatic interactions between the neighboring magnetic particles (which can be justified in section IV). We only considered the magnetic energies of these particles in a two-dimensional external magnetic field ($\boldsymbol{H}$), applied in the plane of these magnetic particles (thin films). The magnetic moments can only rotate within the plane (*i.e.* only the in-plane anisotropy is considered).

The total energy of a single S-W particle as shown in Fig. 1 is given by $E = K_u \sin^2\theta_1 - H m_s \cos(\theta_2 - \theta_1)$, where θ_1 is the angle between the magnetization vector ($\boldsymbol{m}_s$) and the easy-axis of the particle, and θ_2 is the angle between the applied field vector ($\boldsymbol{H}$) and the easy-axis. In the S-W model, the equilibrium direction of $\boldsymbol{m}_s$ of a single particle is obtained by minimizing the total energy of the particle using the criteria $\partial E/\partial\theta_1 = 0$, and $\partial^2 E/\partial^2\theta_1 = 0$. The solutions of these two equations can be obtained by using the Newton-Raphson method[11]. A geometric construction, known as the Asteroid Rule[12–14] (see Fig. 1), is employed to visualize the determination of the equilibrium direction of $\boldsymbol{m}_s$. According to the Asteroid Rule, the equilibrium direction is parallel to one of the lines tangent to the asteroid and passing through the tip of magnetic field vector $\boldsymbol{H}$. When $\boldsymbol{H}$ is inside the asteroid, four tangent lines (shown in grey in Fig. 1) can be drawn and the two possible equilibrium directions are parallel to the two lines making smallest angles with the easy-axis (labeled $\boldsymbol{m}_s$ and $\boldsymbol{m}_s'$ in Fig. 1). When $\boldsymbol{H}$ is outside the asteroid, two such tangent lines can be drawn, and the equilibrium direction is parallel to the one making a smaller angle with respect to the easy-axis. The equilibrium direction changes continuously when $\boldsymbol{H}$ crosses the asteroid curve passing from the inside to the outside regions.

According to the magnetotunneling theory[15], for an MTJ with a sufficiently thick barrier, the electrical conductance (G) can be expressed as a linear function of the cosine of the angle (θ) between the magnetic moments of the free and pinned layers: $G = G_0[1 + P^2\cos\theta]$, where G_0 is a constant, P is the spin polarization of tunneling electrons. If the MR is known for this MTJ (in our case, MR=35%), the spin polarization P can be obtained using the relation: $\mathrm{MR} \equiv \frac{G_P - G_{AP}}{G_{AP}} = \frac{2P^2}{1-P^2}$. Assuming that the magnetization of the pinned layer is fixed(0^o), and that the equilibrium direction of the magnetization of the free layer (θ_F) is derived from the Asteroid Rule, we can compute the field sensitivity by (d is the derivative symbol)

$$s \equiv \frac{1}{G}\cdot\frac{dG}{dH} = \frac{1}{G_0[1+P^2\cos\theta_F]}\cdot\frac{G_0P^2 d(\cos\theta_F)}{dH} = \frac{P^2}{[1+P^2\cos\theta_F]}\cdot\frac{d(\cos\theta_F)}{dH}. \quad (1)$$

Based on the definition of field sensing map described in the previous section, we calculated the sensitivity map of a

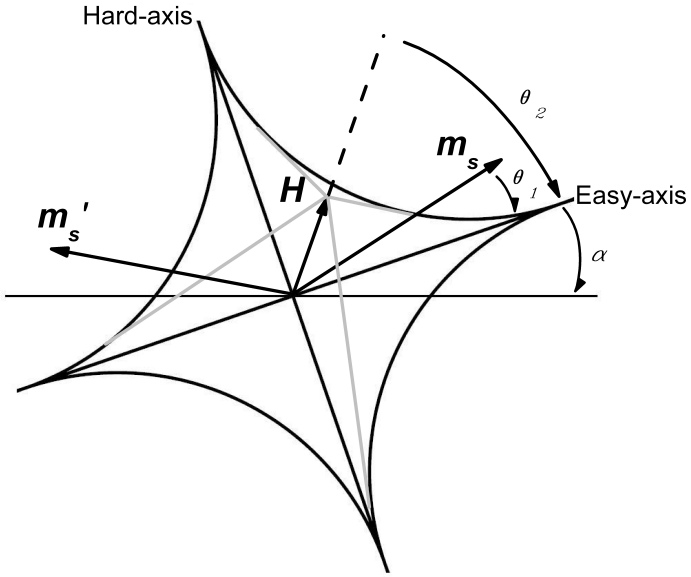

FIG. 1. The Asteroid Rule of the Stoner-Wohlfarth model for a single-domain magnetic particle. Each particle is specified by its magnetic moment $\boldsymbol{m}_s$, anisotropy constant K_u, and easy-axis direction α. θ_1 is the angle between the magnetization vector $\boldsymbol{m}_s$ and the easy-axis of the particle, and θ_2 is the angle between the applied field vector $\boldsymbol{H}$ and the easy-axis. The equilibrium direction of $\boldsymbol{m}_s$ (or $\boldsymbol{m}_s'$) is parallel to one of the lines tangent to the asteroid and passing through the tip of magnetic field vector $\boldsymbol{H}$ (shown in grey).

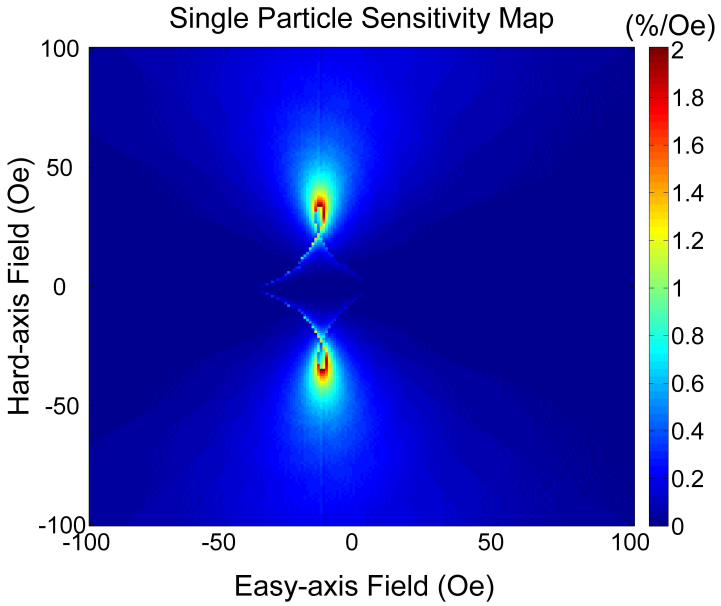

FIG. 2. The simulated sensitivity map for a single-domain magnetic particle. The field sensitivity defined as $s \equiv (1/G)(dG/dH)$ is plotted as a function of easy- and hard-axis fields. The color bar shows the scale of values in the map, and the red spots represent the most sensitive areas, with highest field sensitivity value being 1.91%/Oe. In this simulation, the coercive field is 28 Oe, MR is 35%, and offset from zero on the easy-axis is -13 Oe.

single free layer as shown in Fig. 2. The sharply-confined red spots represent the most sensitive areas of the map, and also mark the boundary between the reversible and irreversible magnetic switchings. The horizontal distance between the two edges of the asteroid (visible in Fig. 2) is twice the coercive force H_c. The centers of the high sensitivity spots are shifted from zero on the easy-axis to about -13 Oe, which is chosen to be consistent with experimental results. The sensitivity map contains rich information, which will be further discussed later.

As mentioned earlier, our MTJ device being studied consists of a collection of magnetic particles, each to be modeled as a single-domain with a unique easy-axis orientation α and anisotropy constant K_u. If we allow dispersions in α and K_u, a composite sensitivity map of an entire MTJ array can be created as a result of the superposition of all thirty-eight individual sensitivity maps. By comparing the simulated sensitivity map to the experimental map, we can extract valuable information such as real coercivity, anisotropy field, and dispersions in α and K_u. In this sense, we applied a Mean-Square-Error (MSE) based image processing method to quantitatively ascertain the degree of similarity between the simulated and the experimental sensitivity maps. In MSE analysis, $\mathbf{x} = \{x_i | i = 1, 2, ..., N\}$ is the experimental map, and $\mathbf{y} = \{y_i | i = 1, 2, ..., N\}$ is one of the many simulated maps with varying magnetic parameters. N is the number of pixels, and x_i and y_i are the pixel intensity of the ith pixels in $\mathbf{x}$ and $\mathbf{y}$, respectively. The MSE between the two maps is defined as MSE($\mathbf{x}$, $\mathbf{y}$) $\equiv \frac{1}{N}\sum_i (x_i - y_i)^2$. We then minimized this MSE number for the two maps, and found the optimal match. This optimization process provided us with the anisotropy dispersion in practical MTJ devices.

IV. RESULTS AND DISCUSSION

We obtained the magnetoresistance ratios (MR) of an MTJ array as the external field, H_E, was varied along the easy-axis of the free layer. As shown in Fig. 3, in the absence of a hard-axis field, a square-shaped hysteresis loop was observed with an MR of 35%. Under a large hard-axis field (60 Oe), the hysteresis loop evolved into a reversible and non-hysteretic curve with an unsaturated MR of 23%. The simulated transfer curves are also plotted with a solid line in the memory configuration (0 Oe), and a dashed line in the sensing configuration (60 Oe). Both of them show good consistency with the experimental results. In the inset a), we showed an image of 38 MTJ junctions in a series array, with adjacent MTJ junctions connected to each other alternately through the bottom or top electrical leads. A scale of 100μm and the direction of easy-axis are also indicated. The magnetic field due to the magnetic dipole moment of adjacent elements can be approximated by $H_d = \frac{\mu_0}{4\pi}\frac{2m_s}{r^3}$, where m_s is the magnetization moment for each element ($\approx 10^{-14}$ emu), and μ_0 is the permeability of free space, r is the distance between adjacent junctions (30$\sim$90 μm). The result shows H_d is in the order of 0.1 Oe, which is well below the applied magnetic field, thus it is reasonable to assume that magnetic coupling between adjacent domains has a minimal effect on the results for large applied fields.

Because of this array configuration, junctions sharing the same bottom leads were measured together. For the 19 pairs of junctions in each device as seen in Fig. 4, left panel, a total of nineteen transfer-curve measurements were carried out to yield the distributions of resistances (in parallel configurations), TMR ratios, coercivities, and offset values from zero on the easy-axis. The resistance for device 1 is therefore about 2.02 KΩ (106.7 $\Omega\times$19).

Due to the deposition process, the resistances, as well as other characteristic parameters for MTJ devices, tend to vary from batch to batch and show a certain degree of variation throughout the wafer surface. However, Fig. 4, left panel shows small deviations for these parameters among the MTJ pillars for a single device, which justifies our assumption that we can use statistical methods to study the magnetic anisotropy dispersion in CoFeB/MgO/CoFeB MTJs. The following discussion is based on the result obtained for device 1, while the results for other devices are qualitatively the same.

Certain defects, such as edge roughness, encourage the formation of edge domains along the boundary of a free layer magnetic element[16]. At the saturated parallel state of an MTJ element, both magnetizations in the interior region of the element (M_i) and the edge domains (M_e) align with the external field. At the remnant state (excluding the effect of Neel coupling), the magnetizations in the edge domains tend to orient themselves away from the magnetization in the interior region depending on the local inhomogeneity, while M_i remains unchanged. This effect may cause the average magnetization vector in the element to deviate slightly from the saturated state, leading to the minor curling at the beginning of the magnetization reversal as evidenced in Fig. 4, right panel.

The possible existence of active edge domains in the magnetic field range of interest (-100 Oe to 100 Oe) gives rise to a model correction term to the magnetization dispersion. This term can be capped by analyzing the TMR curve as shown in Fig. 4, right panel. Since the electrical conductance of an MTJ cell is $G = G_0(1 + P^2 \times \cos(\theta))$, θ is the orientation of magnetization vector in the free layer cell relative to that of the pinned layer, we use the conductance values at A and B (or C and D) to calculate the uncertainty in θ due to the edge domains, the result is about 0.4 degrees. Therefore, our simulation results have an uncertainty of about 0.4 degrees regarding the magnetization dispersion as a result of edge domains. Note the above uncertainty is purely for a single free layer element, and it should not be confused with the distribution of anisotropy axis orientation in multiple MTJ elements in one device

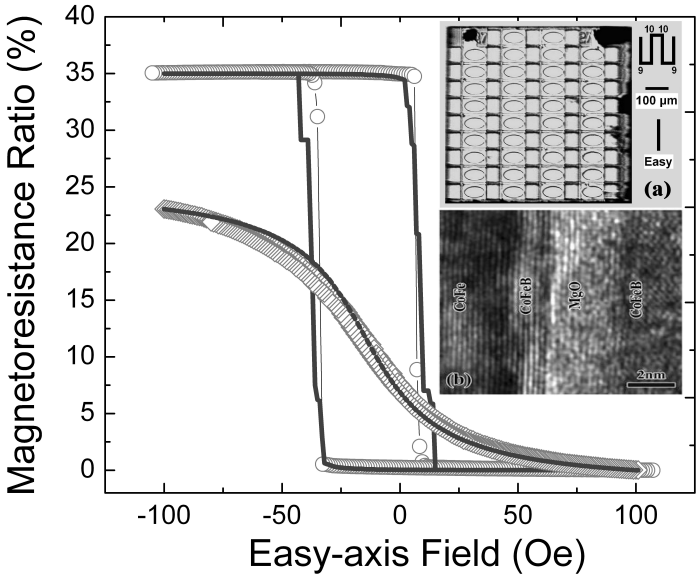

FIG. 3. Magnetoresistance ratios of an MTJ device as the external field is varied along the easy-axis of the free layer. The curve of circles is the experimental data with H_B=0 Oe, and the curve of diamonds is the hysteresis-free response at H_B=60 Oe. The simulated MR curves are also plotted. The inset a) shows an optical image of 38 MTJ sensors in a series array (device 1), with adjacent MTJ sensors connected to each other alternately through the bottom or top electrical leads. The inset b) shows a cross-sectional TEM image of our sample.

(about 4.5 degrees) as will be discussed later.

The experimental sensitivity map plots the sensitivity value as a function of the easy-axis and hard-axis bias fields as seen in Fig. 5. This technique enables us to locate the most sensitive region of an MTJ device by suitably choosing the optimum biasing magnetic fields. There are two high sensitivity spots of around 1.2%/Oe (orange through dark red) peaking at $H_B \sim \pm 30$ Oe and $H_E \sim$-13 Oe. In the region between these spots, the sensitivity drops rapidly and becomes almost zero for $|H_B| <$10 Oe due to the hysteresis behavior of the MTJ. The centers of the high sensitivity spots are shifted from zero on the easy-axis to about -13 Oe. This shift is a manifestation of the coupling between the ferromagnetic (free and pinned) layers. Such a coupling is either due to the direct magnet dipolar coupling between the free layer and pinned layer, or due to the coupling that results from the correlated roughness of the ferromagnetic layers, called Neel or "Orange-Peel" coupling[18,19]. Given that the synthetic-antiferromagnetic pinned layer reduces the magnetostatic interaction between the layers, Neel coupling is thought to be the major source here[7]. This coupling favors a parallel alignment of the layers and has to be overcome by the easy-axis field. It was further confirmed by an analysis of the TEM cross-sectional image as seen in Fig. 3, inset b): using the method described in reference[19], the amplitude and wavelength of the interfacial roughness profile we obtained are about 5 Åand 100 Å, giving an offset value of 12.3 Oe.

As we discussed earlier, the characteristics of a sensitivity map for an array system strongly depends on the following parameters: 1) dispersions in anisotropy angles and anisotropy constants (α, K_u), 2) MR value, 3) coercivity (H_c), and 4) offset from zero on the easy-axis field. To find the simulated sensitivity map for a system made up of multiple MTJ elements, we created a gallery of images with varying parameters 1 through 4. The best matched simulated map is presented in Fig. 6 with a minimized MSE number. In this simulation, the MR is 35%, and the coercive force and offset value are 28 Oe and -13 Oe respectively, which is consistent with values obtained experimentally in Fig. 3. The highest field sensitivity is 1.39%/Oe, which is almost identical to the experimental value. The anisotropy angle α follows a Gaussian distribution with a mean value of 0 and a standard deviation of 0.08 rad ($\sim$4.5 degrees). As opposed to the qualitative approach used in Safron's work[8], where the angular dispersion of anisotropy is said to be proportional to the normalized derivative of the remnant curve, the standard deviation we obtained here has more practical meaning (0.08 rad). On the other hand, for each free layer element, the effective anisotropy constant K_u is correlated with the magnetic moment $\boldsymbol{m_s}$ and the coercive force H_c according to $\frac{2K_u}{m_s H_c} = 1$[13]. If we let m_s and H_c be

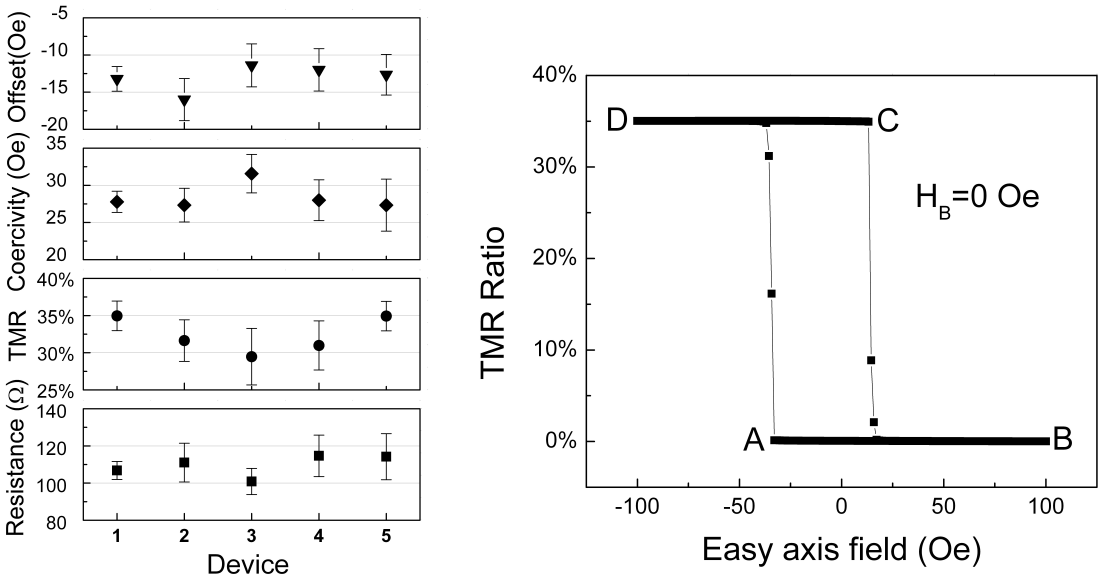

FIG. 4. Left panel: for a total of 5 MTJ devices, distributions of resistance values (parallel state), TMR ratios, coercivities, and offset values are shown, represented by squares, circles, diamonds, and triangles, respectively. Because of the array configuration, no fewer than two MTJ junctions could be measured together, thus each data point shows the mean value and standard deviation for a total of 19 measurements per device. Right panel: TMR curves for a single MTJ element as the applied field is varied along the easy-axis of the free layer in absence of hard axis (H_B) magnetic fields.

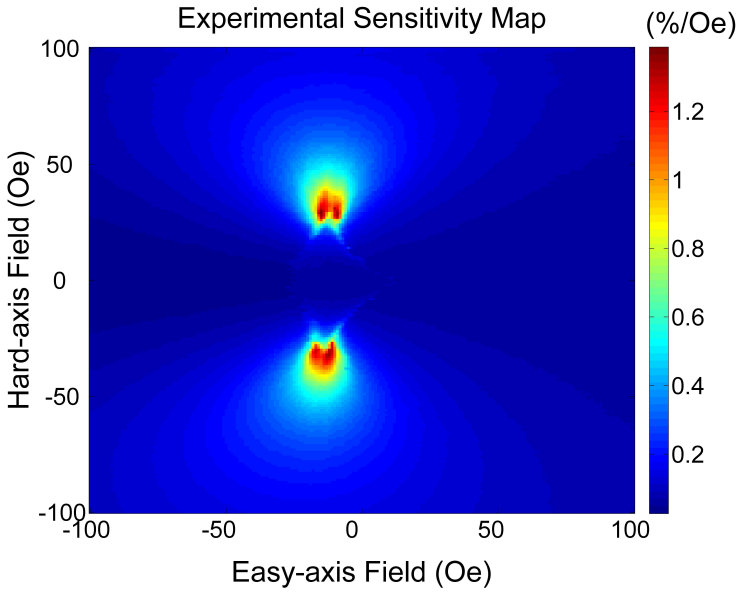

FIG. 5. The experimental sensitivity map of an MTJ array. The sensitivity value is plotted as a function of the easy-axis and hard-axis fields. Two high sensitivity spots are located at $H_B \sim \pm 30$ Oe, $H_E \sim$-13 Oe, with s as high as 1.38%/ Oe. In the region between these spots the sensitivity drops rapidly and becomes almost zero for $|H_B| <$10 Oe.

constant (H_c be the coercive force for the whole system), the variable $\frac{2K_u}{m_s H_c}$ in each element is no longer an identity, but follows a Gaussian distribution. In our case, the distribution has a mean value of 1, and a standard deviation of 0.02.

Although the simulated and the experimental maps show a high degree of similarity, there exist minor differences between them. First, the experimental map is slightly rotated, meaning the pinning direction of MTJ device is not

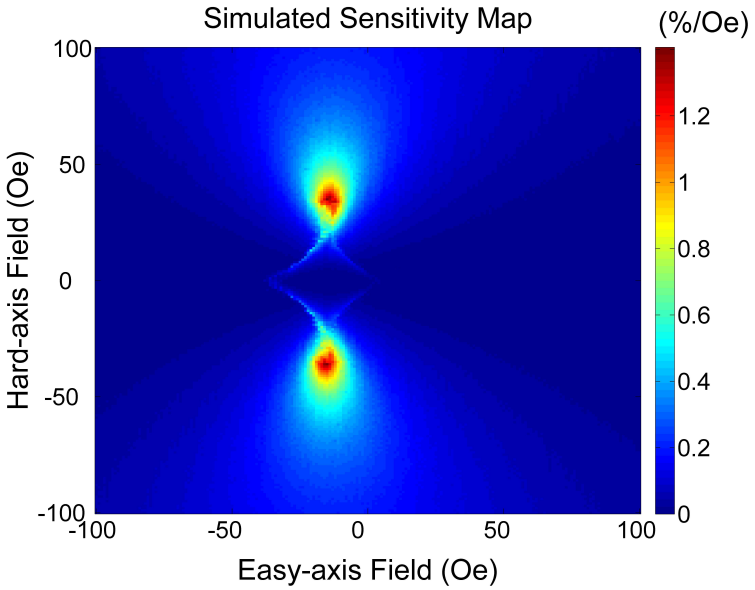

FIG. 6. The simulated sensitivity map of a system made up of multiple magnetic tunnel junctions. The map is plotted as superposition of multiple sensitivity maps, and the parameters used in this map are optimized in order to resemble most of the experimental map. In our case, MR=35%, the coercive field H_c=28 Oe, the offset value=-13 Oe, for anisotropy angle: $\overline{\alpha}$ =0, σ_α =0.08 rad; for anisotropy constant $\frac{\overline{2K_u}}{m_s H_c}$=1, $\sigma(\frac{2K_u}{m_s H_c})$ =0.02. Here H_c stands for the coercive force for the system, not for each element.

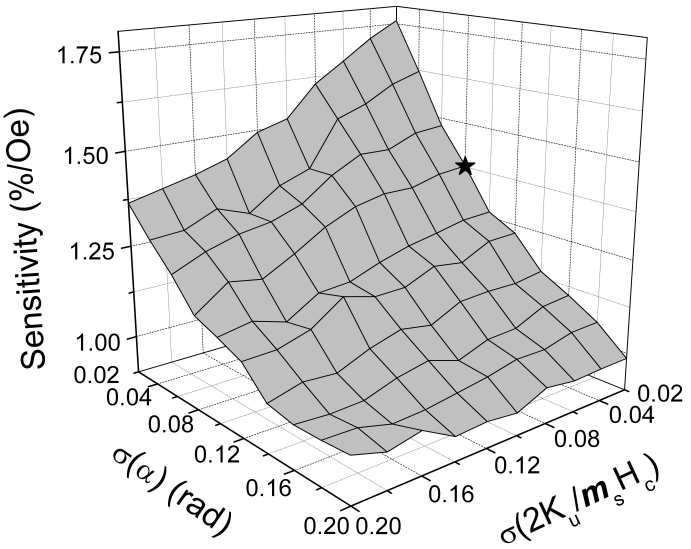

FIG. 7. The field sensitivity (peak value) as a function of anisotropy dispersions: dispersion in anisotropy angle σ_α and dispersion in anisotropy constant, $\sigma(\frac{2K_u}{m_s H_c})$. A contour is made by just varying anisotropy dispersions, with all the other parameters kept the same as in Fig. 6. The field sensitivity always decreases with increased dispersions, and the experimental work is indicated by a star.

perfectly aligned with the easy-axis field H_E. Second, the red spots in the experimental map are less elongated than those in the simulated map. This can be explained by the fact that the magnetization of the pinned layer is slightly re-oriented in the presence of a large hard-axis field, causing field sensitivity s to drop more rapidly with an increasing H_B. This factor was not accounted for in our simulated model.

Since the parameters 1 to 4 depend on the thin film deposition and patterning processes, we studied how the

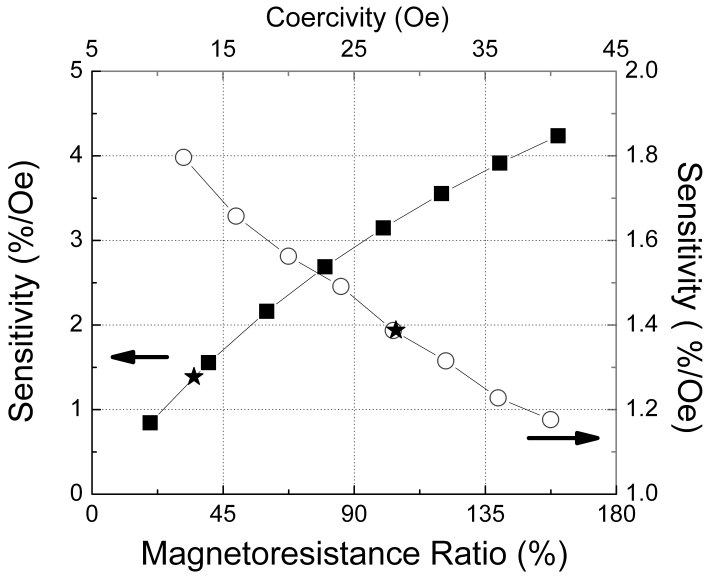

FIG. 8. The field sensitivity (peak value) as functions of magnetoresistance ratio (indicated by the solid squares) and coercive field (indicated by the empty circles). The curves are made with only MR or H_c varying, with all the other parameters remaining the same as in Fig. 6. An increase in MR value can result in a greater sensitivity value, and an increase in H_c can reduce the field sensitivity. The experimental work is marked by a star.

field sensitivity s changes as each of these parameters is varied independently. The purpose is to examine which parameter is more critical to the sensitivity. We first studied the effect of statistical dispersions in anisotropy angles and anisotropy constants. Fig. 7 shows the dependence of sensitivity on the standard deviations of α and K_u, with all other parameters (*e.g.*, MR and coercivity) kept the same as in Fig. 6. The experimental data point is marked by a star on the contour in Fig. 7.

Since the system being studied consists of a collection of free layer elements, each of them has a unique easy-axis orientation α and anisotropy energy constant K_u. The sensitivity map for the system can be viewed as a superposition of multiple single-particle sensitivity maps. A positive change in α will result in a counter-clockwise rotation of a sensitivity map (while a negative change will result in a clockwise rotation). Similarly, a positive change in K_u will expand a sensitivity map (while a negative change will contract a sensitivity map). As the position of the most sensitive area of a single-particle sensitivity map is not necessarily the same as in another map, the sensitive area of the composite map will expand if there are sizeable dispersions of α and K_u in the whole system. Thus, the field sensitivity always decreases with increased dispersions. Physically, a spintronic device often consists of many MTJ elements working in unison, and the dispersions in them cause them to be less responsive to the external magnetic field. To significantly reduce the dispersion, we may consider improving the uniformity throughout the wafers and improving the magnetic annealing process. As shown in Fig. 7, the field sensitivity (peak value on a sensitivity map) drops rapidly as the dispersion in α becomes larger, and less rapidly with an increasing dispersion in $\frac{2K_u}{m_s H_c}$. Sensitivity is almost halved if both dispersions undergo a ten-fold increase.

By keeping the dispersions the same as in Fig. 6, we proceed by varying the MR and coercive force of the array system being studied. Fig. 8 shows the effects of varying MR and coercivity on the field sensitivity (peak value on a sensitivity map). Intuitively, a larger MR value can result in a greater sensitivity value and this can be proved by using the definition of s. Since $s \equiv (1/R)(dR/dH)$, an increase in MR usually leads to an increase in dR/dH over the dynamic range, thus greater field sensitivity is achieved. Precisely speaking, in equation (1), field sensitivity is in positive correlation with the spin polarization P. While P is determined by TMR according to TMR$\equiv \frac{G_P - G_{AP}}{G_{AP}} = \frac{2P^2}{1-P^2}$, or $P = \sqrt{\frac{TMR}{2+TMR}}$. Thus, the relation between MR and s presented in Fig. 8 is well expected. An eight-fold increase in MR can result in a five-fold increase in field sensitivity. The experimental data is marked by a star along the curve for reference.

As for coercivity, the horizontal length of the asteroid in a sensitivity map is twice the coercive force $2H_c$; therefore,

the larger the coercivity, the larger the size of the asteroid. Assuming a unit of easy-axis magnetic field can induce a conductance change ($\triangle G$) at peak spot A (with the highest s value) of an MTJ sensitivity map with the original asteroid, the new sensitivity map, with the coercivity and the size of the asteroid doubled, now requires two units of H_E to make the same conductance change ($\triangle G$) at peak spot A. In other words, dG/dH becomes smaller. Physically, it means that the magnetization of the MTJ device is more rigid, and less responsive to the external magnetic field. This explains the downward trend of the sensitivity as H_c is increased, as shown in Fig. 8. The experimental data is shown by a star along the curve.

Finally, we want to stress that the magnetic field sensitivity is inherently related to the magnetic susceptibility (χ) of an MTJ system. According to the equation (1), the magnetic field sensitivity (s) of an MTJ can be expressed as $s = \frac{P^2}{[1+P^2\cos\theta_F]} \cdot \frac{d(\cos\theta_F)}{dH}$, where d is the derivative symbol, P is the polarization of the spin current, θ_F is the angle between the external magnetic field and the magnetization vector of the free layer, and the pinned layer magnetization is parallel to the external magnetic field applied. Usually the most sensitive use of an MTJ requires that $\theta_F \approx \frac{\pi}{2}$, thus $s \approx \frac{P^2}{m_s} \cdot \frac{d(m_s\cos\theta_F)}{dH} = \frac{P^2}{m_s} \cdot \chi$, here m_s is the saturated magnetic moment. If we know the polarization of spin current and the magnetic moment, we can derive χ from the experimentally obtained field sensitivity. The sensitivity map is therefore directly related to the magnetic susceptibility map. In this sense, an investigation into the sensitivity map of MTJ devices can reveal some fundamental physical behaviors (magnetic dynamics, spin polarization, etc.) of the underlying magnetic elements in micro- to nano-scale.

V. CONCLUSIONS AND SUMMARY

A vector hysteresis modeling method based on the Stoner-Wohlfarth model was developed to account for the anisotropy dispersion in the sensitivity maps of magnetic tunnel junction arrays. We considered the system to be composed of non-interesting single-domain magnetic particles, with each having its own easy-axis and anisotropy constant. By superposing the sensitivity maps of those magnetic particles, we extracted the anisotropy dispersions of practical MTJ arrays by comparing their experimental sensitivity maps to the optimized simulated maps. In addition, we studied the dependence of the field sensitivity value s on magnetoresistance ratio, coercive field, and statistical dispersions of anisotropy parameters. It can be shown that the field sensitivity always decreases with increased dispersions, increases with greater MR value, and decreases with an increasing H_c. It is estimated that the edge domains contribute about 8% (0.4 out of 4.5 degrees) to the magnetization dispersion. We believe that this model is a useful tool for monitoring the formation and evolution of anisotropy dispersion in MTJ arrays, and can facilitate better design of MTJ-based devices.

ACKNOWLEDGMENTS

We would like to thank B. D. Schrag for helpful discussions. At Brown University, the work was supported by National Science Foundation (NSF) under Grant No. DMR-0907353 and by JHU MRSEC under Grant No. DMR-0520491. At Micro Magnetics, Inc., the work was supported by National Science Foundation under Grant No. IIP-0924685.

* wenzhe_zhang@brown.edu
† gang_xiao@brown.edu

[1] J. Hayakawa, S. Ikeda, Y.M. Lee, F. Matsukura, and H. Ohno, Appl. Phys. Lett., **89**, 232510 (2006).
[2] Y.M. Lee, J. Hayakawa, S. Ikeda, F. Matsukura, and H. Ohno, Appl. Phys. Lett., **90**, 212507 (2007).
[3] X. Y. Liu, C. Ren, and G. Xiao, J. Appl. Phys., **92**, 4722 (2002).
[4] C. Albon, A. Weddemann, A. Auge, K. Rott, and A. Hutten, Appl. Phys. Lett., **95**, 023101 (2009).
[5] P. W. T. Pong, B. Schrag, J. Shapiro, R. D. McMichael, and J. W. F. Egelhoff, J. Appl. Phys., **105**, 07E723 (2009).
[6] B. Negulescu, D. Lacour, F. Montaigne, A. Gerken, J. Paul, V. Spetter, J. Marien, C. Duret, and M. Hehn, J. Appl. Phys., **95**, 112502 (2009).
[7] D. Mazumdar, W. F. Shen, X. Y. Liu, B. D. Schrag, M. Carter, and G. Xiao, J. Appl. Phys., **103**, 113911 (2008).
[8] N. S. Safron, D. Schrag, X. Liu, W. Shen, D. Mazumdar, M. J. Carter, and G. Xiao, J. Appl. Phys., **103**, 033507 (2008).
[9] E. C. Stoner and E. P. Wohlfarth, Philos. Trans. R. Soc., London, **240**, 599 (1948).
[10] R. O'Handley, *Modern Magnetic Materials: Principles and Applications* (Wiley-Interscience, 2000).
[11] C. S. Koh and S. Y. Hahn and G. S. Park, IEEE Trans. Magn., **36**, 1254 (2000).
[12] I. D. Mayergoyz, *Mathematical Model of Hysteresis* (Springer-Verlag, 1990).
[13] A. Ivanyi, *Hysteresis Models in Electromagnetic Computation* (Akademia Kiado, Budapest, 1997).
[14] E. C. Stoner and E. P. Wohlfarth, IEEE Trans. Magn., **27**, 3475 (1991).
[15] J. C. Slonczewski, Phys. Rev. B, **39**, 6995 (1989).
[16] D. Meyners, H. Bruckl, and G. Reiss, J. Appl. Phys., **93**, 2676 (2002).
[17] N. Shimomura, T. Kishi, M. Yoshikawa,E. Kitagawa,Y. Asao,H. Hada,H. Yoda, and S. Tahara, IEEE Trans. Magn., **41**, 2652 (2005).
[18] L. Neel, Acad. Sci., Paris, **255**, 1545 (1962).
[19] B. D. Schrag, A. Anguelouch, S. Ingvarsson, G. Xiao, Y. Lu, P. L. Trouilloud, A. Gupta, R. A. Wanner, W. J. Gallagher, P. M. Rice, and S. S. P. Parkin, Appl. Phys. Lett., **77**, 2373 (2000).